Article

A Flexible Wearable Strain Sensor Based on Nano-Silver Modified Laser-Induced Graphene for Monitoring Hand MovementsCitation: To Be Added by Editorial Staff during Production

Mian Zhong *, Yao Zou, Hongyun Fan, Shichen Li, Yilin Zhao, Bin Li, Bo Li, Yong Jiang, Xiaoqing Xing, Jiaqing Shen, Chao Zhou *

Posted Date: 1 July 2024

doi: 10.20944/preprints202407.0026.v1

Keywords: LIG; doping modification; silver nanoparticles; flexible wearable strain sensor; single-step in situ

Article

A Flexible Wearable Strain Sensor Based on Nano-Silver Modified Laser-Induced Graphene for Monitoring Hand Movements

Mian Zhong [1,†,*], Yao Zou [1,†], Hongyun Fan [1], Shichen Li [1], Yilin Zhao [2], Bin Li [2], Bo Li [3], Yong Jiang [4], Xiaoqing Xing [1], Jiaqing Shen [1] and Chao Zhou [1,*]

[1] Institute of Electronic and Electrical Engineering, Civil Aviation Flight University of China; Deyang 618307,China, mianzhong@cafuc.edu.cn (M.Z.); zouyao670427@163.com (Y.Z.);18731838513@163.com (H.F.); lscxy19990217@163.com (S.L.); xingxiaoqing@cafuc.edu.cn (X.X.); shenjiaqing@cafuc.edu.cn (J.S.); zc_cafuc@163.com(C.Z.)

[2] Faculty of Chemical Engineering, Kunming University of Science and Technology, Kunming 650500, China;zhaoyl@stu.kust.edu.cn(Y.Z.); kmlb@vip.sina.com(B.L.)

[3] School of Physics, University of Electronic Science and Technology of China, Chengdu 611731, China; libcx@uestc.edu.cn(B.L.)

[4] School of Mathematics and Physics, Southwest University of Science and Technology, Mianyang 621010, China; y_jiang@swust.edu.cn (Y.J.)

* Correspondence: mianzhong@cafuc.edu.cn (M.Z.);zc_cafuc@163.com;

† These authors contributed equally to this work.

Abstract: The advancement of performance in the domain of flexible wearable strain sensors has become increasingly significant due to extensive research on laser-induced graphene (LIG). An innovative doping modification technique is required owing to the limited progress achieved by adjusting laser parameters to enhance LIG's performance. By pre-treating with $AgNO_3$, we successfully manufactured LIG with a uniform dispersion of silver nanoparticles across its surface. The experimental results for the flexible strain sensor exhibit exceptional characteristics, including low resistance (183.4 Ω), high sensitivity (426.8), a response time of approximately 150 ms, and a relaxation time of about 200 ms. Moreover, this sensor demonstrates excellent stability under various tensile strains and remarkable repeatability during cyclic tests lasting up to 8,000 s. Additionally, this technique yields favorable results in finger bending and hand back stretching experiments, holding significant reference value for preserving the inherent characteristics of LIG preparation in a single-step and in situ manner.

Keywords: LIG; doping modification; silver nanoparticles; flexible wearable strain sensor; single-step in situ

1. Introduction

With the advancement of science and technology, the limitations of traditional wearable devices are becoming increasingly apparent. These limitations include their bulky size, poor data accuracy, and inability to meet users' demands for portability and precise monitoring. In this context, flexible wearable devices have emerged as a compact, simple solution capable of providing more accurate and diverse physiological monitoring functions [1]. Current research on flexible wearable strain sensors primarily focuses on designing innovative materials such as Mxene [2], conductive hydrogels [3], and graphene [4], which are used to prepare highly sensitive sensors for detecting human physiological signals and movements. Among these materials, graphene [5] stands out due to its exceptional optical, electrical, and mechanical properties, which make it a revolutionary material for future applications [6].

Graphene preparation methods include chemical gas deposition [7], liquid phase separation [8], and epitaxial growth [9]. However, these methods often involve complexity and high costs. The

 doi:10.20944/preprints202407.0026.v1

method of laser-induced graphene (LIG) is notable for its simplicity and low cost [10]. LIG exhibits excellent conductivity, mechanical flexibility, and environmental stability. It possesses a three-dimensional porous structure that makes it ideal for flexible wearable strain sensors. The properties of LIG are influenced by various factors such as the type of carbon precursor [11–13], laser parameters [14–16], and doping modifications [17,18], which can significantly impact performance. Thus, it is crucial to study these influencing factors and select appropriate materials and parameters to achieve high-performance LIG.

The main research directions involve systematic investigations of laser parameters and doping modification experiments on LIG. By exploring the effect of the laser on the carbon precursor surface, we can understand the evolution of LIG's microstructure [19]. Additionally, controlling laser parameters allows for the regulation of LIG's microstructure and surface characteristics during preparation, leading to optimized performance [20]. However, studying LIG's performance remains a challenge. Doping modification provides a means to enhance or improve specific properties of LIG, thereby expanding its potential applications in flexible wearable strain sensors. Current research primarily focuses on introducing target objects such as Pt [21], MoS2 [22], and carbon nanotubes [23] to enhance specific properties. However, this approach increases experimental complexity and can introduce instability and inconsistency into the preparation process. Therefore, optimizing doping technology can achieve significant performance improvements and promote the widespread application of LIG in flexible wearable strain sensors.

Based on our previous study [24,25], we propose the concept of introducing nano-Ag particles with excellent conductivity into LIG through a single-step preparation process. By pre-treating the carbon precursor polyimide (PI) to incorporate Ag ions onto its surface, nanometer-sized silver particles are doped into the generated LIG via laser-induced experiments. Subsequently, we investigate the effects of doped Ag^+ on LIG characteristics, performance, and application in flexible wearable sensors. The main innovations and contributions of this study can be summarized as follows:

1. We propose a nano-Ag modified LIG flexible wearable strain sensor, which offers a novel approach for the in situ, single-step preparation of LIG and the fabrication of high-performance flexible sensors.
2. The nano-Ag modified LIG flexible strain sensor exhibits exceptional characteristics, including low resistance, superior sensitivity, excellent stability, and remarkable repeatability.
3. The high-performance flexible wearable strain sensor can accurately characterize the finger bending angles. Additionally, based on its exceptional electric heating performance, it can be further expanded to the field of hand heating and insulation for pilots in cold environments, providing a more comfortable and safe flight experience for pilots.

2. Materials and Methods

2.1. Preparation of LIG

The experimental process for the preparation of doped silver nanoparticles with uniform distribution in LIG is illustrated in Figure 1. Initially, a 125 μm-thick polyimide (PI) film (Shenzhen Jihongda Plastic Products Co., Ltd., CHN) is immersed in deionized water and subjected to ultrasonic cleaning for 10 min using an ultrasonic cleaner (Chun Rain Inc., Shenzhen, CHN). The PI film is then dried at a constant temperature of 50°C for 30 min in a heat and constant drying oven (Shaoxing Subo Instrument Co., Ltd., CHN). Subsequently, sodium hydroxide (NaOH) is dissolved in ionized water within a beaker and mixed thoroughly using a magnetic stirrer to prepare a NaOH solution with a concentration of 2.5 mol/L. The PI film is then immersed in the NaOH solution, which leads to the breakdown of imide groups on its surface and the formation of polyamide acid along with sodium salt. Subsequently, the PI film is immersed in $AgNO_3$ solutions with concentrations of 0.01, 0.03, and 0.05 mol/L respectively, each for 30 min, to replace Na ions from the sodium salts with Ag ions from the $AgNO_3$ solution. After each immersion, the film is cleaned and dried with ionized water. For the laser experiments, the treated PI film is securely fixed on a three-dimensional mobile platform and exposed to a Synrad P150 CO_2 infrared laser (Novanta Corporation, USA). It is important to note that

 doi:10.20944/preprints202407.0026.v1

temperatures exceeding 300°C during the salt preparation process may lead to the decomposition of silver ions, resulting in the formation of individual silver atoms. However, for LIG production and generation through laser experiments, a significantly higher temperature threshold (>300°C) is required. This facilitates the breakdown of individual silver atoms while doping LIG with nanometer-sized silver particles.

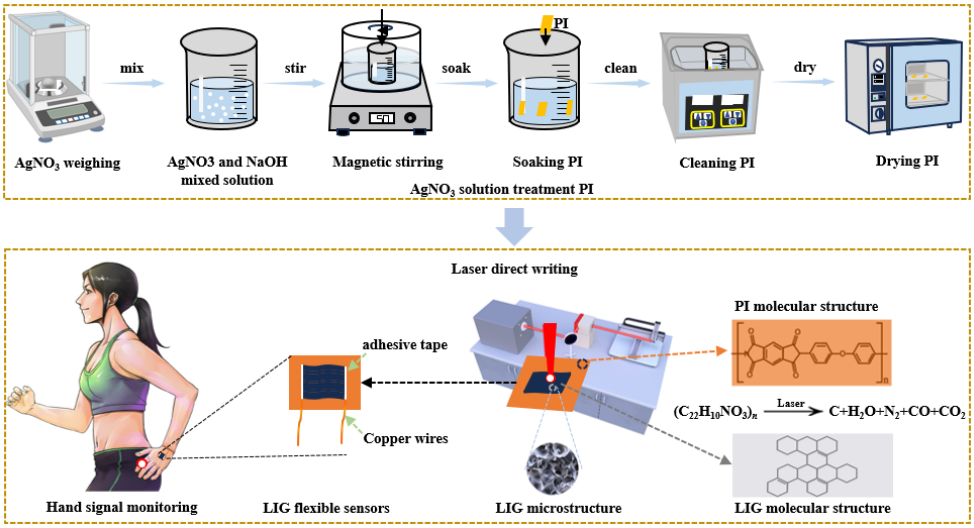

Figure 1. Experimental process of LIG.

3. Results and Discussion

3.1. Surface Morphology of LIG

The surface morphology analysis of Ag-x/LIG, generated using different concentrations of $AgNO_3$ solution, was conducted. Figure 2 presents the SEM image of Ag-x/LIG, facilitating microscopic observation of the LIG surface. In Figure 2(a), both a sample diagram and an SEM image were obtained from untreated PI, serving as a control. SEM magnification reveals that the surface of LIG is smooth with no visible grains. Figure 2(b) displays the samples and SEM images of Ag-0.01/LIG, revealing small particle distributions on the surface caused by the laser radiation energy impacting the PI surface, and the silver is analyzed at high temperature(>300°C). Figure 2(c) shows the Ag-0.03/LIG sample along with its SEM image, demonstrating a slightly denser distribution of silver nanoparticles compared to those on the Ag-0.01/LIG surface. This increased density may be attributed to the higher concentration of $AgNO_3$, facilitating more extensive ion exchange processes, thereby promoting LIG formation as active sites during the laser action experiments at elevated temperatures and resulting in larger nano-silver particle formation.

However, Figure 2(d) illustrates the SEM image of Ag-0.05/LIG, revealing that the elemental silver particles on its surface is less conspicuous than those depicted in Figure 2(c). This discrepancy can be attributed to the more complete reaction of PI induced by Ag^+ during laser experimentation, resulting in an increased generation of LIG. The abundant three-dimensional pore structure of LIG disperses elemental silver particles, reducing their visibility on the surface area of LIG. Thus, Ag-0.03/LIG may exhibit superior quality in this experimental setup.

 doi:10.20944/preprints202407.0026.v1

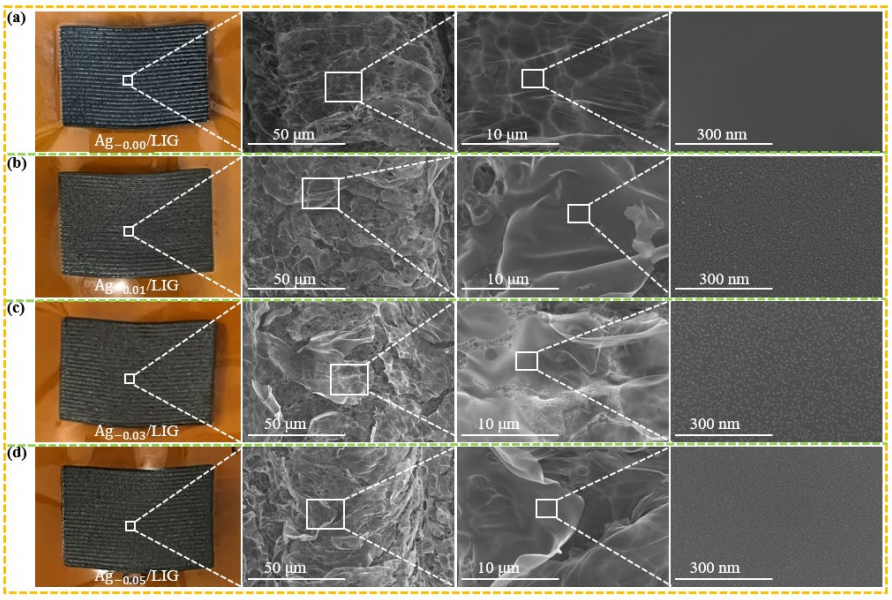

Figure 2. SEM detection of Ag-x/LIG. (a) Ag-0.00/LIG, (b) Ag-0.01/LIG, (c) Ag-0.03/LIG, (d) Ag-0.05/LIG.

Therefore, SEM and EDS were employed to test the Ag-0.03/LIG samples, and the corresponding results are presented in Figure 3. The SEM image depicted in Figure 3(a) reveals a uniform distribution state of the LIG surface, while the elemental spectrum analysis from Figure 3(b)–(f) also confirms the presence of nanoparticles within the LIG.

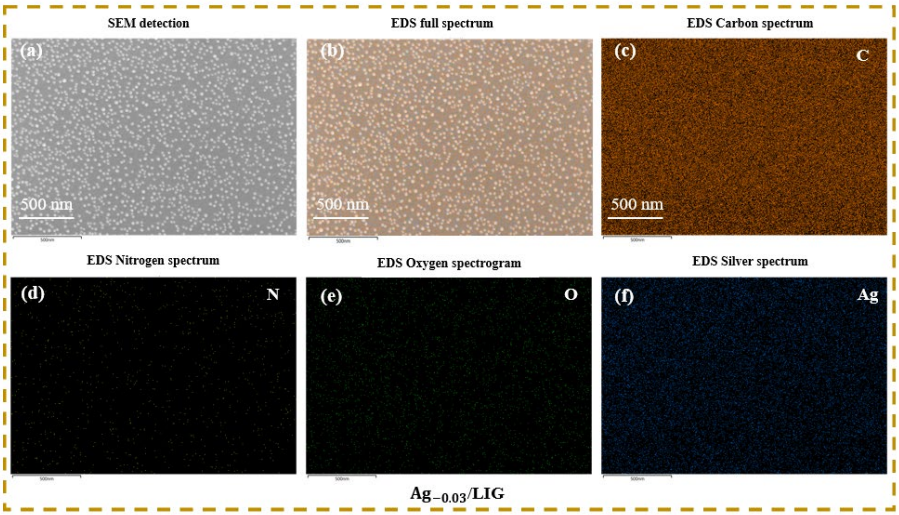

Figure 3. SEM and EDS detection of Ag-0.03/LIG. (a) SEM detection, (b)-(f) Full spectrum and partial spectrum of EDS.

3.2. Characterization of LIG

Raman and XRD tests were conducted for Ag-0.00/LIG, Ag-0.01/LIG, Ag-0.03/LIG, and Ag-0.05/LIG samples. The results are depicted in Figure 4. Figure 4(a) presents the Raman analysis of LIG at varying concentrations [26], showing the D peak at 1333.62 cm^{-1}, G peak at 1576.53 cm^{-1}, and 2D peak at 2678.79 cm^{-1}. The intensities of these peaks were analyzed to obtain the I_D/I_G ratio depicted in Figure 4(b). A higher I_D/I_G ratio indicates more defects in LIG due to the addition of nano silver from increasing concentrations of the $AgNO_3$ solution used during the synthesis process. The I_{2D} and I_G values both exceed unity, suggesting that LIG is multilayered. Figure 4(c) displays the XRD analysis of LIG, used to analyze the crystal structure. The Ag ions modified LIG exhibits a prominent (002)

 doi:10.20944/preprints202407.0026.v1

peak at 2θ = 24.98°, corresponding to the characteristic peak of graphene [27], and a weak (100) peak at 2θ = 44.02°, which corresponds to the arrangement of aromatic rings in the carbon material. These distinct peaks confirm the presence of graphene. Additionally, Figure 4(d) reveals the crystal faces (111), (200), (220), and (311) at angles of 38.04°, 47.16°, 64.4°, and 77.84°, respectively [28], indicating high purity elemental silver content in the LIG.

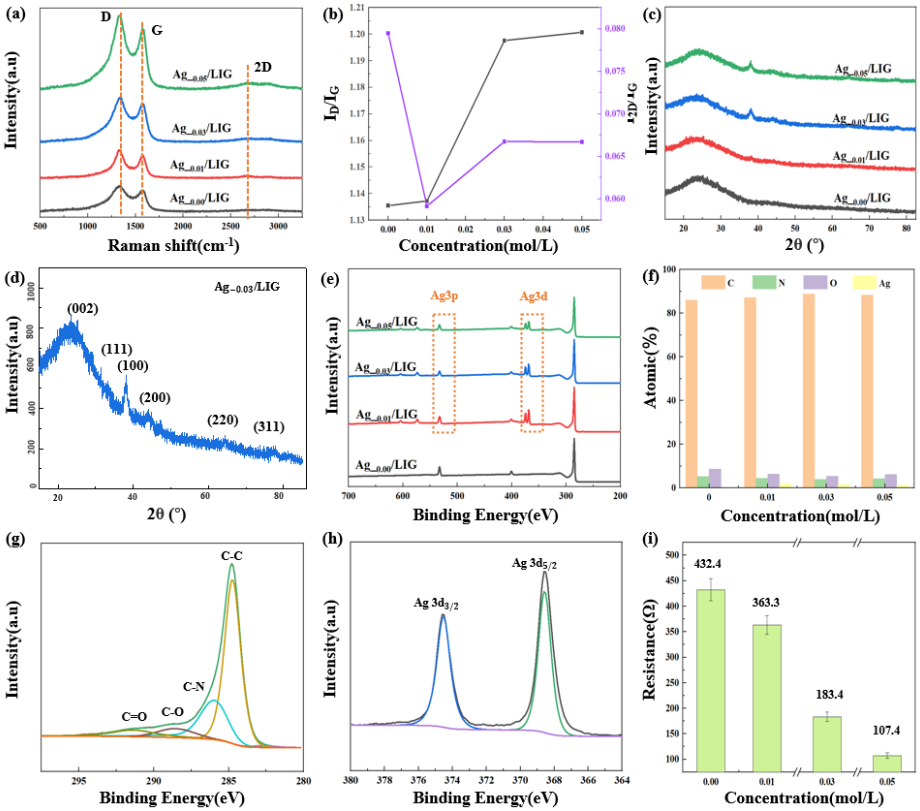

Figure 4. Characterization of Ag-x/LIG. (a) Raman spectra, (b) Calculation value of I_D/I_G and I_{2D}/I_G, (c) XRD detection, (d) Detection of Ag-0.03/LIG, (e) XPS detection, (f) Element content percentage, (g) C1s sub-peak and fitting, (h) Ag3d sub-peak and fitting, (i)Resistance of Ag-x/LIG.

XPS analysis was also performed for all concentrations to determine the element species and content of LIG, as shown in Figure 4(e). The results exhibited the presence of C, N, and O elements for all samples. Compared to Ag-0.00/LIG, the XPS spectra of Ag-0.01/LIG, Ag-0.03/LIG, and Ag-0.05/LIG displayed additional peaks corresponding to Ag3d and Ag3p. The atomic percentage composition of C, N, O, and Ag in LIG at different concentrations is presented in Figure 4(f). Notably, Ag-0.00/LIG contains no silver elements, whereas Ag-0.01/LIG, Ag-0.03/LIG, and Ag-0.05/LIG all contain Ag. The C1s peak of Ag-0.03/LIG can be divided into four sub-peaks: C=C, C-N, C-O, and C=O, as shown in Figure 4(g) [29]. Similarly, the Ag3d peak is divided into two peaks: Ag3d3/2 and Ag3d5/2, demonstrated in Figure 4(h). The flexible wearable strain sensor based on Ag-x/LIG underwent initial resistance tests with different concentrations of $AgNO_3$. As depicted in Figure 4(i), a decreasing trend in resistance was observed as the concentration of $AgNO_3$ increased, with recorded values of 432.4 Ω, 363.3 Ω, 183.4 Ω, and 107.4 Ω, respectively. These findings suggest that increasing the concentration of $AgNO_3$ solution enhances the reduction in the resistance value of the sensor.

3.3. Performance Testing of Doping Ag-LIG Sensor

The sensitivity of the flexible wearable strain sensor reflects its ability to detect minute changes in the external environment, specifically its response to applied strain, which is a critical parameter for assessing the sensor's performance and directly impacts its effectiveness and accuracy in practical

 doi:10.20944/preprints202407.0026.v1

applications. The Gauge factor (GF) of the sensor, which indicates sensitivity, is calculated based on the relative resistance change and tensile strain:

$$GF = \frac{\delta(R - R_0) / R_0}{\delta\varepsilon} \quad (1)$$

where GF represents the sensitivity factor of the sensor, R is the real-time resistance of the sensor, R0 is the initial resistance, $(R - R_0) / R_0$ is the relative resistance change of the sensor, and δε is the tensile strain of the sensor.

Performance testing and evaluation of flexible wearable strain sensors, based on Ag-x/LIG prepared with varying concentrations of $AgNO_3$ following PI pretreatment, were conducted as shown in Figure 5. Figure 5(a) explores the strain-relative resistance response characteristics of four distinct samples. Figure 5(b) focuses on the relative resistance changes of the Ag-0.03/LIG-based flexible wearable strain sensor, employing a three-stage function for fitting. The sensitivity factor GF of the sensor was found to be 37.2 within the 0%–5% tensile strain range in the first section. In the second section, a significant increase in the sensitivity factor GF to 177.3 was observed within the 5.0%–8.0% range. Moreover, as the tensile strain further increased to 8.0%–11%, an even higher sensitivity factor GF value of 426.8 was achieved. Figure 5(c) compares the performance among four types of flexible wearable strain sensors, revealing that Ag-0.03/LIG-based sensors exhibit superior GF values. Additionally, as illustrated in Figure 5(d), our sensor demonstrates exceptional sensitivity compared to other materials or processes utilized for the preparation of flexible wearable strain sensors [17,30–38].

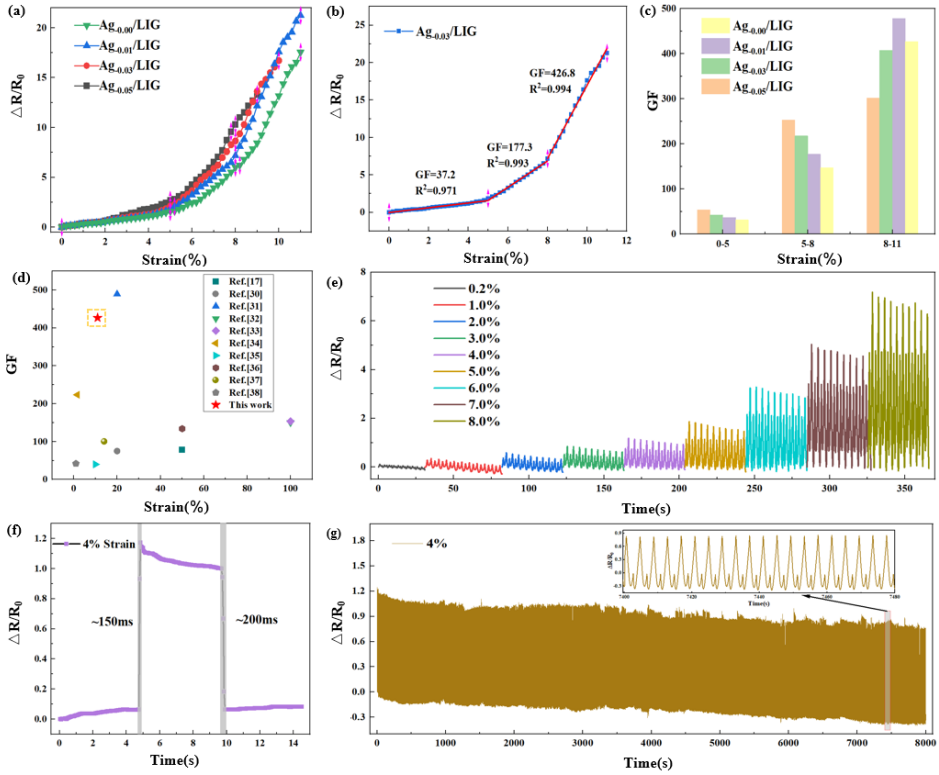

Figure 5. Tensile performance tests of the flexible wearable strain sensor. (a) Tensile strain and relative resistance tests, (b) Tensile strain and relative resistance change test of Ag-0.03/LIG-based flexible wearable strain sensor, (c) Sensitivity comparison of four flexible wearable strain sensors, (d) Sensitivity comparison of Ag-0.03/LIG-based flexible wearable strain sensors with other materials or processes, (e) Stability testing at different tensile lengths, (f) Time response testing, (g) Cyclic repeatability testing.

In Figure 5(e), the stability test results of the flexible wearable strain sensor under various tensile strains are presented. The experimental results demonstrate that the sensor has an impressive detection limit as low as 0.2%. Moreover, it has been subjected to ten cycles of testing across a range

 doi:10.20944/preprints202407.0026.v1

of tensile strains from 1.0% to 8.0%, at intervals of 1.0%, showcasing exceptional stability. Figure 5(f) illustrates the time response characteristics of the flexible wearable strain sensor, revealing a response time of approximately 150 ms and a relaxation time of around 200 ms when subjected to a tensile strain of 4.0% for a duration of 5 s at a speed of 500 mm/s, before being released at the same speed. Additionally, cyclic repeatability testing was conducted on the sensor, demonstrating excellent repeatability over an extended period lasting up to 8000 s. These comprehensive test results highlight the sensor's rapid response and high stability, making it highly suitable for applications that require utmost reliability and prompt feedback.

3.4. Application of Ag-LIG Sensor

The flexible wearable strain sensor offers a broad range of applications across various sectors. Specifically, the relative resistance waveform of the sensor demonstrates corresponding patterns. To further explore the variation in relative resistance and the maximum testing angle of the flexible wearable strain sensor under different degrees of bending, this study conducted an analysis, with findings presented in Figure 6. The initial step involved attaching the sensor to the inner side of a hinge to simulate finger flexion at various bending angles. As shown in Figure 6(a), when the hinge bends, the sensor also bends outwardly along with its protruding LIG surface, leading to changes in the conductive path and subsequent alterations in relative resistance. Bending was performed at 30° intervals, starting from 0° and maintained at each angle for approximately 15 s up to a maximum bend angle of 120°. Subsequently, the bend was gradually released at equal intervals. The relative changes in resistance were measured as depicted in Figure 6(b), demonstrating that similar variations occur within identical bending angles for this device. The results underscore the sensor's effective measurement capability across various levels of finger flexion, while maintaining excellent stability and reversibility characteristics. Figure 6(c) illustrates θ as a reliable parameter for quantifying finger flexion angles, and Figure 6(d) depicts the relative resistance changes associated with utilizing this device to assess such angles. Notably, there is an incremental increase in resistance with every additional 15° increment in bending. The change in relative resistance of the flexible wearable strain sensor is depicted in Figure 6(e) as it is subjected to force while being attached to the back of the hand. The gripometer encompasses seven weight categories, ranging from a minimum of 5 kg to a maximum of 60 kg. Notably, an increase in the gripometer's gravity scale corresponds to an elevation in the relative resistance exhibited by the sensor. Therefore, it can be concluded that this versatile and adaptable technology provides valuable insights into accurately measuring finger flexion angles.

Preprints.org (www.preprints.org) | NOT PEER-REVIEWED | Posted: 1 July 2024 doi:10.20944/preprints202407.0026.v1

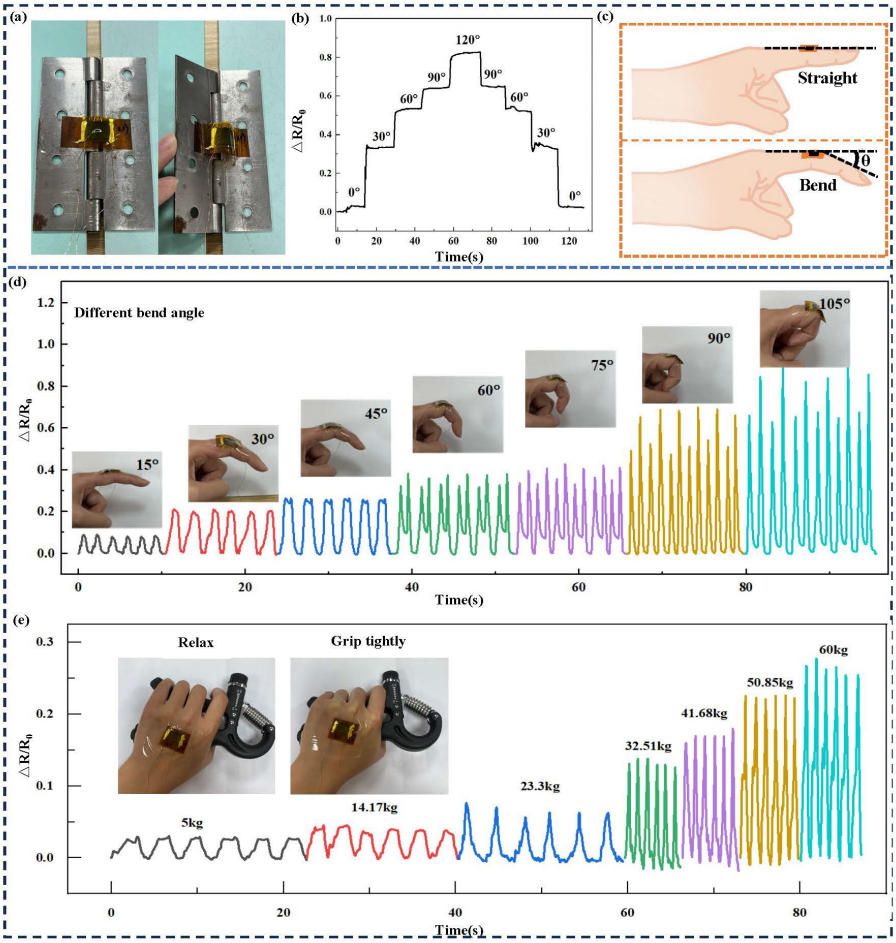

Figure 6. Changes in relative resistance of flexible wearable strain sensors under different tensile forces.

The infrared thermal imager was employed for real-time monitoring of the Ag-0.03/LIG-based flexible wearable strain sensor to evaluate temperature variations and electric heating performance, as illustrated in Figure 8. The graph in Figure 7(a) demonstrates a continuous increase in maximum surface temperature with incremental voltage increases, reaching a peak of 119.2°C at a setting of 10 V. Figure 7(b) provides a direct assessment of the temporal and voltage-dependent changes in surface temperature, clearly showing an increasing maximum temperature as the voltage rises. Simultaneously, different voltages induce a rapid initial temperature rise within the first 10 s, followed by significantly reduced fluctuations that converge toward stability thereafter. By examining Figure 7(c), it is observed that at a voltage of 2 V, the surface temperature of the sensor approximates the ambient temperature (28.8°C). As the voltage gradually increases, there is a corresponding increase in the maximum surface temperature until it reaches its final value at 10 V (146.4°C). Figure 8(d) demonstrates an upward correlation between the surface temperature of the Ag-0.03/LIG-based flexible wearable strain sensor and the applied voltage. Furthermore, when comparing flexible wearable strain sensors based on Ag-0.03/LIG and LIG, it becomes apparent that nano silver enhances conductivity and reduces heating time due to its excellent electrical conductivity properties. The enhanced heat generation can be attributed to the infiltration of nano silver into the three-dimensional nanopore structure of LIG, effectively reducing overall resistance and enhancing current conduction efficiency within the material.

 doi:10.20944/preprints202407.0026.v1

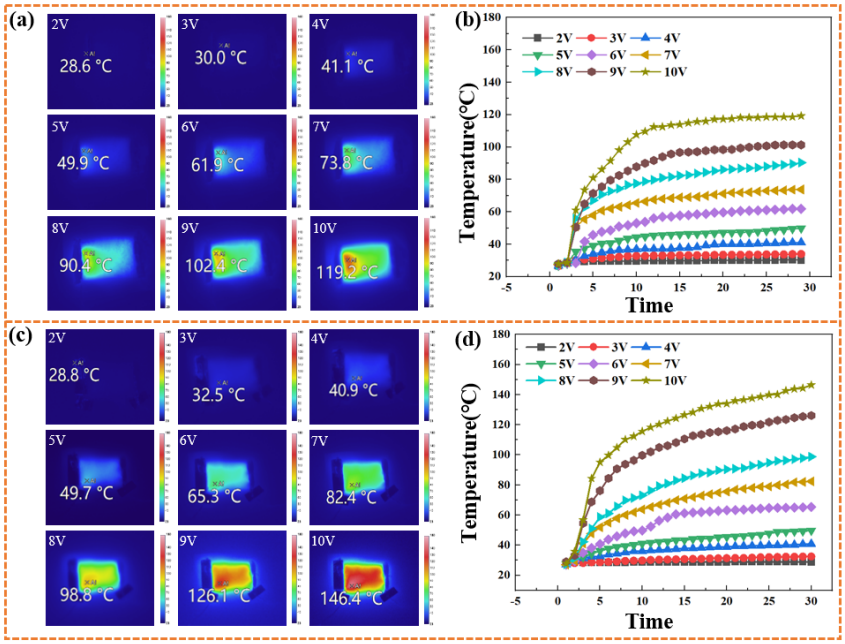

Figure 7. Thermal performance test and temperature change curve of LIG-based and Ag-0.03/LIG-based flexible wearable strain sensor. (a) Infrared thermal performance test of LIG, (b) Temperature change curve during the electric heating performance test of LIG, (c) Infrared thermal performance test of Ag-0.03/LIG, (d)Temperature change curve during the electric heating performance test of Ag-0.03/LIG.

The excellent electric heating performance of the flexible wearable strain sensor enables its extensive application. It can be utilized not only for pilot flight training in indoor simulators at normal temperatures or for monitoring other human physiological signals, but also for hand warming and maintenance in cold environments. In extremely low temperatures, pilots may experience adverse effects on their manual dexterity and response time due to compromised finger flexibility, potentially compromising flight safety. The integration of flexible wearable strain sensors into gloves or hand-worn devices, along with the utilization of their electric heating function, enables the provision of continuous and comfortable hand warming to pilots during flights. The implementation of this solution effectively alleviates the discomfort caused by cold conditions on pilots' hands, thereby enhancing hand comfort and reaction speed. Ultimately, this contributes significantly to ensuring flight safety.

4. Conclusions

This study aimed to enhance the characteristics of LIG through Ag doping modification. The PI substrate was pretreated with $AgNO_3$ solutions at concentrations of 0.01, 0.03, and 0.05 mol/L to introduce Ag ions onto its surface, followed by laser experiments. The SEM, XRD, and XPS analyses revealed the presence of uniformly distributed silver nanoparticles on the LIG surface. Tensile performance testing demonstrated that the Ag-0.03/LIG-based flexible sensor exhibited the highest sensitivity, reaching 426.8, representing a significant improvement compared to the undoped LIG-based flexible sensor. The subsequent performance tests confirmed the sensor's outstanding stability and repeatability, suggesting its potential application in specific fields for experimental verification and practical use. This experiment provides a novel approach for the in situ preparation of LIG and the fabrication of high-performance sensors in a single step.

Author Contributions: Conceptualization, methodology, data curation, and writing—original draft preparation, M.Z. and Y.Z.; supervision, writing—review and editing, and funding acquisition, M.Z. and C.Z.; resources, validation, formal analysis, H.F., and S.L.; visualization, investigation, Y.Z., and B.L.; data curation, B.L.;

validation, Y.J.; conceptualization, X.X.; methodology, J.S.; All authors have read and agreed to the published version of the manuscript.

Funding: The authors gratefully acknowledge the financial support from the Key Laboratory of Flight Techniques and Flight Safety,CAAC(FZ2022ZZ03), the General Project of Sichuan General Aircraft Maintenance Engineering and Technology Research Center (GAMRC2021YB12), and Research Project of Fund Project for Basic Scientific Research Expenses of Central Universities (24CAFUC03020).

Institutional Review Board Statement: Not applicable.

Informed Consent Statement: Not applicable.

Data Availability Statement: Data sharing is not applicable to this article.

Acknowledgments: Not applicable.

Conflicts of Interest: The authors declare no conflict of interest.

References

1. Chen, H., Zhuo, F., Zhou, J., et al. Advances in graphene-based flexible and wearable strain sensors. *Chem. Eng. J.*, **2023**, 464: 142576.
2. Yang, R., Song, H., Zhou, Z., et al. Ultra-sensitive, multi-directional flexible strain sensors based on an MXene film with periodic wrinkles. *ACS Appl. Mater. Interfaces*, **2023**, 15(6), 8345-8354.
3. Song, Y., Niu, L., Ma, P., et al. Rapid preparation of antifreezing conductive hydrogels for flexible strain sensors and supercapacitors.*ACS Appl. Mater. Interfaces*, **2023**, 15(7), 10006-10017.
4. Yuan, L., Gao, X., Kang, R., et al. Flexible strain sensors based on an interlayer synergistic effect of nanomaterials for continuous and noninvasive blood pressure monitoring. *ACS Appl. Mater. Interfaces*, **2024**, 16(20): 26943–26953.
5. He, S., Wu, J., Liu, S., et al. A fully integrated multifunctional flexible sensor based on nitrile rubber/carbon nanotubes/graphene composites for smart tire. *Chem. Eng. J.*, **2024**, 486: 150104.
6. Gao, Y., Wang, Y. Interplay of graphene–DNA interactions: Unveiling sensing potential of graphene materials. *Appl. Phys. Rev.*, **2024**, 11: 011306.
7. Pirabul, K., Zhao, Q., Sunahiro, S., et al. A thermodynamically favorable route to the synthesis of nanoporous graphene templated on CaO via chemical vapor deposition. *Green Chem.*, **2024**, 26(10): 6051-6062.
8. Zong, H., Gao, M., Mohsan A., et al. Effect of static pressure on ultrasonic liquid phase exfoliation of few-layer graphene. Ultrason. Sonochem., **2024**, 105:106863.
9. Park, J., Yuhyeon, O., Yang, M., et al. Nanoscale mapping of relativistic photocarrier transports in epitaxial graphene surface and edge states. *Carbon*, **2024**, 226: 119162.
10. Li, Z. H., Huang, L.B., Cheng L., et al. Laser-induced graphene-based sensors in health monitoring: Progress, sensing mechanisms, and applications. *Small Methods*, **2024**: 2400118.
11. Cheng, J. F., Tang, S. Q., Wang, Z. L., et al. Design of high-performance bilayer solar evaporator using graphene-coated bamboo prepared by near-infrared laser-induced carbonization of polystyrene. *Adv. Mater. Technol-US*, **2023**, 9(1): 2301211.
12. Luo, Y., Zhu, B. C., Zhang, S. Y., et al. Stretchable and flexible non-enzymatic glucose sensor based on poly(ether sulfone)-derived laser-induced graphene for wearable skin diagnostics. *Adv. Mater. Technol-US*, **2022**, 7(9): 2101571.
13. Zhang, Q., Qu, M. L., Liu, X. Y., et al. Three-in-one portable electronic sensory system based on low-impedance laser-induced graphene on-skin electrode sensors for electrophysiological signal monitoring[J]. *Adv. Mater. Interfaces*, **2022**, 10(3): 2201735.
14. Liu, H. L., Zheng, Y. X., Moon, K. S., et al. Ambient-air in situ fabrication of high-surface-area, superhydrophilic, and microporous few-layer activated graphene films by ultrafast ultraviolet laser for enhanced energy storage. *Nano Energy*, **2021**, 94: 106902.
15. Sujit, D., Kalyan, G., Martin, P., et al. Laser-induced MXene-functionalized graphene nanoarchitectonics-based microsupercapacitor for health monitoring application. *ACS Nano*, **2023**, 17(20): 20537-20550.
16. Liu, H. W., Chen, K. S., Wu, R. M., et al. Laser-induced graphene-based flexible substrate with photothermal conversion and photoresponse performance on polyimide film. *ACS Appl. Mater. Interfaces*, **2023**, 15(39): 46550-46558.
17. Liu, W., Chen, Q., Huang, Y. H., et al. In situ laser synthesis of Pt nanoparticles embedded in graphene films for wearable strain sensors with ultra-high sensitivity and stability. *Carbon*, **2022**, 190: 245-254.
18. Zhang, Q. W., Zhang, F. Y., Liu, X., et al. Doping of laser-induced graphene and its applications[J]. *Adv. Mater. Technol-US*, **2023**, 8(16): 2300244.

19. Roche, J. D. L., López-Cifuentes, I., Jaramillo-Botero, A., Influence of lasing parameters on the morphology and electrical resistance of polyimide-based laser-induced graphene(LIG). *Carbon Lett*, **2022**, 33(2): 587-595.
20. Karimi, G., Lau, I., Fowler, M., et al. Parametric study of laser-induced graphene conductive traces and their application as flexible heaters. *Int. J. Energ. Res.*, **2021**, 45(9): 13712-13725.
21. Robert, G. H., Cícero, C. P., Raquel, R. A. S., et al. Laser-induced graphene decorated with platinum nanoparticles for electrochemical analysis of saliva. *ACS Appl. Nano Mater.*, **2023**, 6(22): 20801-20811.
22. Thuy, N. T. D., Zhao, G., Wang, X. C., et al. Potassium ion-selective electrode with a sensitive ion-to-electron transducer composed of porous laser-induced graphene and MoS_2 fabricated by one-step direct laser writing. *Electroanal.*, **2022**, 35(3): e202200194.
23. Chen, J. Y., Ling, Y. H., Yuan, X. M., et al. Highly sensitive detection of formaldehyde by laser-induced graphene-coated silver nanoparticles electrochemical sensing electrodes. *Langmuir*, **2023**, 39(36): 12762-12773.
24. Zou, Y., Zhong, M., Li, S. C., et al. Flexible wearable strain sensors based on laser-induced graphene for monitoring human physiological signals. *Polymers*, **2023**, 15(17): 3553.
25. Xing, X., Zou, Y., Zhong, M., et al. A Flexible wearable sensor based on laser-induced graphene for high-precision fine motion capture for pilots. *Sensors*, **2024**, 24: 1349.
26. Zhu, C. C., Lu, Q. T., Ying, W., et al. Graphene oxide humidity sensor with laser-induced graphene porous electrodes. *Sensor Actuat B-Chem.*, **2020**, 325: 128790.
27. He, M. H., Wang, G. T., Zhu, Y. X., et al. In-situ joule heating-triggered nanopores generation in laser-induced graphene papers for capacitive enhancement. *Carbon*, **2021**, 186: 215-226.
28. Qin, W. F., Geng, J. H., Lin, C. X., et al. A flexible strain sensor based on MXene/AgNW composite film with extremely high sensitivity and low strain range for real-time health monitoring and thermal management. *J. Phys. D Appl. Phys.*, **2023**, 56(19): 195401.
29. Alexandre, F. C., António, J. S. F., Cátia, L., et al. Laser-induced graphene strain sensors produced by ultraviolet irradiation of polyimide. *Adv. Funct. Mater.*, **2018**, 28(52): 1805271.
30. Yang, H. R., Wang, S. G., Huang, Q. M., et al. Stretchable strain sensor based on HfSe2/LIG composite with high sensitivity and good linearity within a wide range. *Appl. Surf. Sci.*, **2023**, 636: 157772.
31. Tang, L., Zhou, J. Y., Zhang, D. W., et al. Laser-induced graphene electrodes on poly(ether–ether–ketone)/PDMS composite films for flexible strain and humidity sensors. *ACS Appl. Nano Mater.*, **2023**, 6(19): 17802-17813.
32. Wang, H., Zhao, Z. F., Liu, P. P., et al. A soft and stretchable electronics using laser-induced graphene on polyimide/PDMS composite substrate. *npj Flex. Electron.*, **2022**, 6(1): 26.
33. Cheng, X., Cai, J., Xu, J. H., et al. High-performance strain sensors based on Au/graphene composite films with hierarchical cracks for wide linear-range motion monitoring. *ACS Appl. Mater. Interfaces*, **2022**, 14(34): 39230-39239.
34. Wang, W. T., Lu, L. S., Lu, X. Y., et al. Scorpion-inspired dual-bionic, microcrack-assisted wrinkle based laser induced graphene-silver strain sensor with high sensitivity and broad working range for wireless health monitoring system. *Nano Res.*, **2022**, 16(1): 1228-1241.
35. Alexander, D., Kirill, K., Harald, F., et al. Stretchable and skin-conformable conductors based on polyurethane/laser-induced graphene. *ACS Appl. Mater. Interfaces*, **2020**, 12(17): 19855-19865.
36. Liu, F., Wang, G. T., Ding, X. L., et al. Multifunctional laser-induced graphene enabled polymeric composites. *Compos. Commun.*, 2021, 25: 100714.
37. Yang, X. R., Gui, J. H., Dong, C. Q., et al. Laser-induced graphene for screen-printed strain sensors. *ACS Appl. Nano Mater.*, **2023**, 6(23): 21679-21687.
38. Bohdan, K., Beatriz, F. R. S., Alexandre, F. C., et al. Laser-induced graphene from paper for mechanical sensing. *ACS Appl. Mater. Interfaces*, **2021**, 13(8): 10210-10221.